

**Finite Element Method for Designing Plasma Reactors**  
Leo Kempel, Paul Rummel, Tim Grotjohn, and John Amrhein  
Department of Electrical and Computer Engineering  
Michigan State University

**Abstract**

The finite element method has proven to be versatile in the analysis of various electromagnetic phenomena. In this paper, we investigate the utility of the finite element method for guiding the design of plasma reactors. These reactors are used for processing integrated circuit substrates. The design of such reactors is based on the complex interactions between the electromagnetic fields and a plasma-filled region. The reactor geometry, the feed mechanism, and the current state of the plasma determine the electromagnetic fields. This paper investigates the details and difficulties of modeling plasmas within a closed cavity.

**Introduction**

The finite element-boundary integral method has been used in the electromagnetics analysis community for more than two decades, especially for electrostatics and magnetostatics analysis. Solution of dynamic problems, such as antenna characterization, radar cross section calculation, and closed cavity analysis, require the introduction of edge-based (also known as vector) finite elements. However, even with the use of vector finite elements, implementations of a hybrid finite element method were scarce and limited in their utility.

Hybrid finite element methods utilize a boundary integral to close the finite element mesh by providing the relationship between the tangential electric and magnetic fields on the surface of the mesh. The boundary integral explicitly couples each unknown (or edge) on the surface to all the other unknowns resulting in a fully-populated matrix. Hence, this hybrid finite element-boundary integral (FE-BI) method had limited utility in an era of Intel 386-based computers with up to 32 MB of RAM. Fortunately, for modeling plasma-loaded cavities, the feed coaxial aperture requiring a boundary integral is of limited extent and hence results in a relatively light memory demand. However, the relatively large volume of a plasma reactor results in a large number of unknowns to characterize the electric field within the cavity. This led to an intractable computational demand for average plasma reactor users even five years ago.

As computer resources have improved (today, one can purchase a dual processor computer with 1 GB of RAM for less than \$10,000) making what was once called a supercomputer available to average users. Significant effort has been spent over the past few years to make user-friendly computer programs that allow significant simulation capability with a minimal user effort. Specifically, computer program designers are utilizing triangular surface meshes and either right prism or tetrahedra meshes to solve rather complex electromagnetic design problems.

This paper presents the formulation, problem to be solved, and preliminary results for plasma reactor cavities.

## Hybrid Finite Element-Boundary Integral Method

The FE-BI equations ([1],[2]) for a total electric field formulation may be written as

$$\int_V [\nabla \times \mathbf{W}_i \cdot \bar{\bar{\mu}}_r^{-1} \cdot \nabla \times \mathbf{W}_j] dV - k_0^2 \int_V [\mathbf{W}_i \cdot \bar{\bar{\epsilon}}_r \cdot \mathbf{W}_j] dV + jk_0 \int_{S_R} \left[ \frac{(\hat{\mathbf{n}}_R \times \mathbf{W}_i) \cdot (\hat{\mathbf{n}}_R \times \mathbf{W}_j)}{R_e} \right] dS - k_0^2 \int_{S_a} \int_{S_a} [\mathbf{W}_i \cdot \hat{\mathbf{z}} \times \bar{\bar{G}}_{e2} \times \hat{\mathbf{z}} \cdot \mathbf{W}_j] dS' dS = \mathbf{f}_i^{\text{int}} + \mathbf{f}_i^{\text{ext}}$$

where the first term is associated with the curl of the basis function (the magnetic field), the second term is associated with the basis function itself (the electric field), the third term is necessary to account for any resistive transition conditions present (e.g to model thin dielectrics such as glue), and the last term on the left-hand side is the boundary integral term (involving a second kind electric field dyadic Green's function). As shown, the placement of the material parameters ( $\bar{\bar{\epsilon}}_r, \bar{\bar{\mu}}_r$ ) suggests that the basis functions ( $\mathbf{W}_j$ ) and test functions ( $\mathbf{W}_i$ ) should be chosen so that the dot products with the material tensors are accomplished readily. The basis functions presented herein were chosen to accomplish this goal.

An additional observation is that the boundary integral term does not involve the material parameters. Accordingly, since the basis functions and test functions are functionally identical (e.g. Galerkin's testing procedure was used) and the dyadic Green's function is symmetric,  $G_{e2}^{xy} = G_{e2}^{yx}$  and  $\bar{\bar{G}}_{e2}(\mathbf{r}, \mathbf{r}') = \bar{\bar{G}}_{e2}(\mathbf{r}', \mathbf{r})$ , then the boundary integral sub-matrix is symmetric. Therefore, it is not necessary to store either the lower or upper triangle of that matrix.

On the other hand, since it is desirable to allow for the possibility of anisotropic materials within the computational volume, the sparse finite element matrix should be stored without symmetry considerations. Accordingly, it is recommended that the finite element and boundary integral matrices be stored separately and hence that an iterative solver (e.g. BiCG, CG, GMRES) be used. The most significant source of computational cost in an iterative solver is the matrix-vector multiply. This operation can be accomplished with separate matrix storage by realizing

$$\begin{bmatrix} A_{BB} + Y_{BB} & A_{BI} \\ A_{IB} & A_{II} \end{bmatrix} \begin{Bmatrix} E_B \\ E_I \end{Bmatrix} = \begin{bmatrix} A_{BB} & A_{BI} \\ A_{IB} & A_{II} \end{bmatrix} \begin{Bmatrix} E_B \\ E_I \end{Bmatrix} + \begin{bmatrix} Y_{BB} & 0 \\ 0 & 0 \end{bmatrix} \begin{Bmatrix} E_B \\ E_I \end{Bmatrix}$$

where "A" matrices denote finite element interactions and the "Y" matrix indicates the boundary integral matrix. The subscript "B" denotes a boundary edge while "I" indicates an interior edge. This decomposition of the finite element and boundary integral matrices allows the computer program designer to use optimized matrix storage and multiplication schemes for each portion.

Another common aspect to these hybrid finite element computer programs is the need for a volumetric mesh. If tetrahedra are used for the volume mesh, a commercial mesh generating package such as SDRC IDEAS may be used. However, for many applications, an extruded mesh will work perfectly well without the need for additional investment. Extrusion is accomplished by forming elements for each layer of the mesh by replicating the nodal distribution of the top layer for all lower layers of the mesh. Hence, to form the first layer of elements, the top layer nodes are replicated at the interface of the first and second layer. Elements are formed from those nodes (and the previous layer's "bottom"

nodes) and edges are then formed based on the chosen finite element such as right prisms. Such meshes are fairly rigid and hence cannot represent the wide range of geometries that can be modeled using a free mesh (such as that produced by SDRC IDEAS); however, they are often sufficient and considerably simplifies the analysis procedures.

Vector edge-based expansion functions used for right prisms are developed by multiplying the traditional Rao-Wilton-Glisson (RWG) basis function [3] with a function of the prism height for the transverse (e.g. x- and y-component) functions. The normal functions are simply the node-based simplex basis function (see for example [4]) multiplied by  $\hat{z}$ . Hence, the transverse basis functions for edges on the top of the prism are given by

$$\mathbf{W}_\chi = \left( \frac{z}{\Delta z} \right) \mathbf{S}_k = \left( \frac{z}{\Delta z} \right) \frac{d_i}{2S^e} [(x - x_i)\hat{y} - (y - y_i)\hat{x}] \quad \chi = 1,2,3$$

where  $\chi$  is the local edge number and  $i$  is the global edge number. Note that the local edge numbers are defined so that the edge is opposite the local node number as shown in Figure 1.

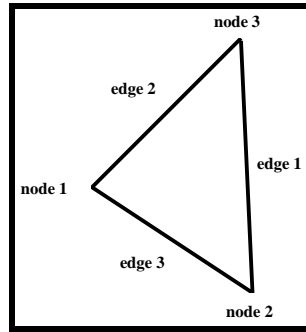


Figure 1. Illustration of local node and edge numbering for a triangle.

Transverse expansion functions on the bottom of the prism are given by:

$$\mathbf{M}_\chi = \left( \frac{\Delta z - z}{\Delta z} \right) \mathbf{S}_k = \left( \frac{\Delta z - z}{\Delta z} \right) \frac{d_i}{2S^e} [(x - x_i)\hat{y} - (y - y_i)\hat{x}] \quad \chi = 4,5,6$$

Finally, the normal (z-directed) expansion functions are given by:

$$\mathbf{K}_\chi = \hat{z} \frac{(x_{k1}y_{k2} - x_{k2}y_{k1}) + (y_{k1} - y_{k2})x + (x_{k2} - x_{k1})y}{2S^e} \quad \chi = 7,8,9$$

where the indices  $k1$  and  $k2$  are given in the following table

$\chi$	$k1$	$k2$
7	2	3
8	3	1
9	1	2

As stated previously, the choice of basis functions is dictated by the physical constraints of the geometry, the requirements for representation of a field, and convenience for implementation. The later

consideration is understood by considering a version of the basis functions given in Chapter 5 of [2]. In that presentation, the basis functions are represented in a *local coordinate system* rather than the *global* treatment given above. Although the solutions are identical, inclusion of anisotropic materials is more difficult if the basis functions are expressed in local coordinates since a transformation back to global coordinates is required to perform the necessary dot products. Hence, the form of the basis functions given above is more convenient for implementation than the form given in [2].

### Plasma Reactors

Plasma reactors are closed cavities energized by high power microwaves to form the desired plasma that is used to perform a desired processing procedure [5]. Figure 2 illustrates Michigan State University's plasma reactor design.

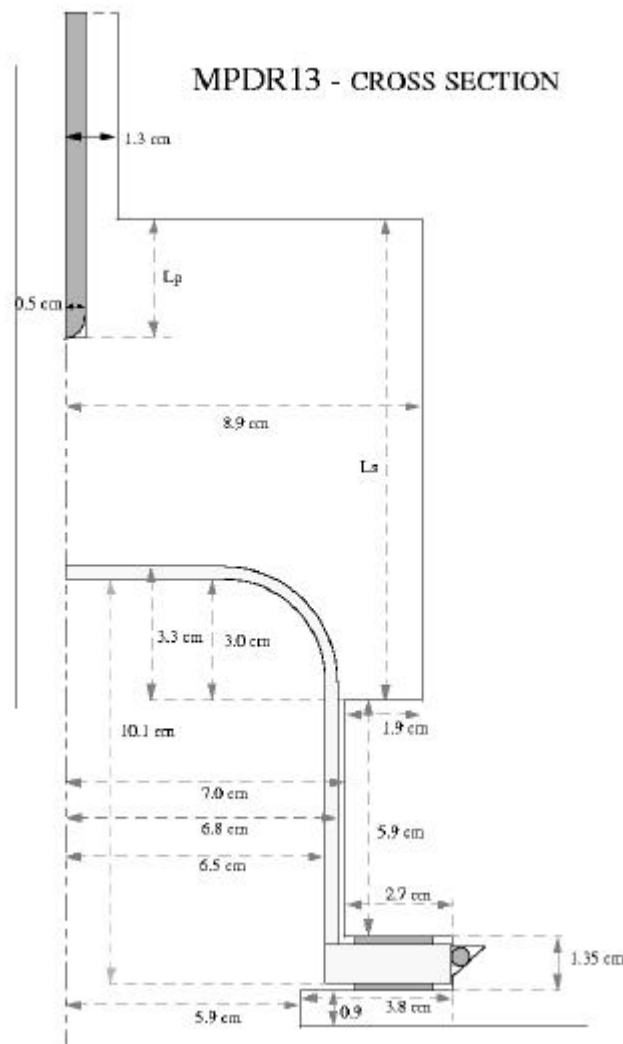


Figure 2. Plasma reactor design used at Michigan State University. (Compliments of Mark Perrin)

This reactor is constructed of brass with adjustable cavity height ( $L_s$ ), adjustable probe length ( $L_p$ ), and a quartz bell jar to contain the plasma formed by a high power microwave source tuned to 2.45 GHz.

The design challenge is to determine the cavity length and probe length so that the maximum energy is coupled to the plasma. The resonant frequency of the cavity is determined by the cavity dimensions as well as the material within the cavity. For our case, the cavity fill is comprised of air, quartz, and plasma. The finite element method is ideal for including this inhomogeneous material fill.

Plasma is formed by the excitation of the cavity by a high power microwave source. This plasma is very difficult to characterize due to the complex physics associated with plasmas as well as its non-stationary behavior. However, we assume that the time scale associated with the evolution of the plasma is much longer than the time it takes to form standing waves within the reactor. Hence, we can assume the reactor state is stationary and consider the plasma in its various excitation states separately.

For our investigation, we are assuming isotropic plasma whose dielectric parameters are given by

$$\epsilon_r = 1 + \frac{\omega_p^2}{-\omega^2 + j\omega\nu}$$

where the plasma frequency is given by  $\omega_p = \sqrt{Ne^2/(m\epsilon_0)}$ ,  $N$  is the electron density, and  $\nu$  is the collision frequency responsible for dampening. We note that for a conducting medium,

$$\epsilon_r = 1 - j \frac{\sigma}{\omega\epsilon_0}$$

which leads to the equivalent conductivity ( $\sigma$ ) of

$$\frac{\sigma}{\epsilon_0} = \frac{\omega_p^2}{\nu + j\omega}$$

Note that unless  $\omega \ll \nu$ , the conductivity is a function of frequency.

Depending on the state of the plasma, it can have a dielectric constant that is greater than zero, less than zero, and even zero! This leads questions as to the conditioning of the finite element matrix as the plasma evolves into its various states. We will discuss our findings regarding modeling plasma at the meeting.

To test our cavity model, including the finite probe thickness, we simulated the  $TM_{012}$  fields within a closed cavity of the dimensions shown in Figure 2 where  $L_s = 14.4$  cm. Figure 3 illustrates the change in resonance frequency as the probe length ( $L_p$ ) is changed. Figure 4 illustrates the axial fields at the base of the cavity (where the plasma will form) at 2.474 GHz.

### Closing Remarks

In this paper, we have presented the finite element method and an application of the method to the design of plasma reactors. The finite element method permits the simulation of a closed cavity with all of the important physics. The plasma reactor's structure, quartz bell jar, plasma load, and feed probe is

included in the model. An extruded right prism mesh is utilized to simplify the analysis task. Results for various configurations will be presented at the conference.

### References

- [1] J.M. Jin and J.L. Volakis, "A hybrid finite element method for scattering and radiation by microstrip patch antennas and arrays residing in a cavity, *IEEE Trans. Antennas Propagat.*, **39**, pp. 1598-1604, Nov. 1991.
- [2] J.L. Volakis, A. Chatterjee, and L.C. Kempel, Finite Element Method for Electromagnetics, New York: *IEEE Press*, 1998.
- [3] S.M. Rao, D.R. Wilton, and A.W. Glisson, "Electromagnetic scattering by surfaces of arbitrary shape," *IEEE Trans. Antennas Propagat.*, **30**, pp. 409-418, May 1982.
- [4] O.C. Zienkiewicz and R.L. Taylor, The Finite Element Method, 4<sup>th</sup> Ed., New York: *McGraw-Hill*, 1989.
- [5] J. Asmussen, T.A. Grotjohn, P. Mak, and M.A. Perrin, "The design and application of electron cyclotron resonance discharges," *IEEE Trans. Plasma Sci.*, **25**, pp. 1196-1221, 1997.

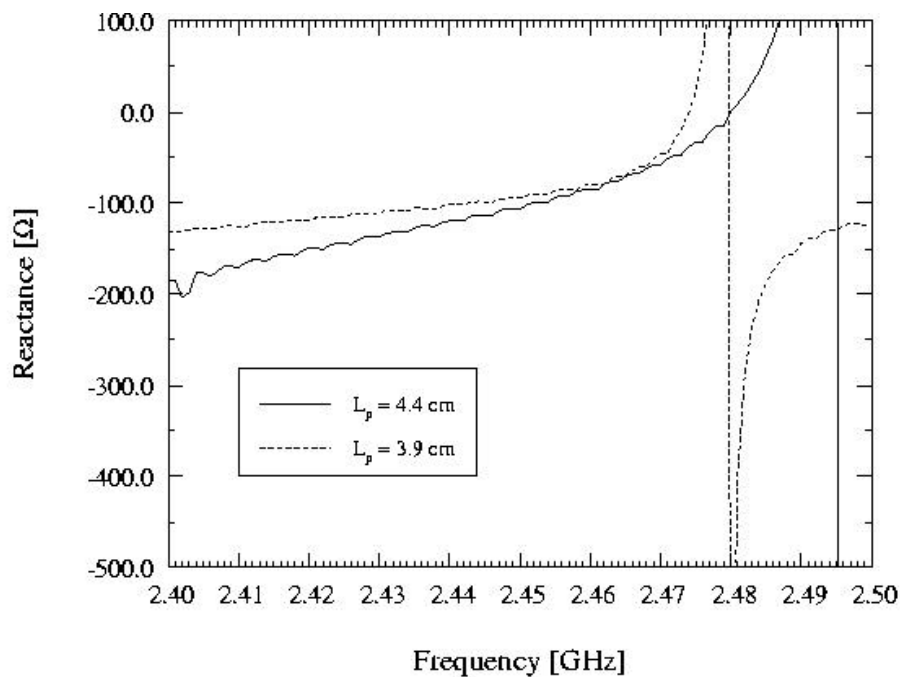


Figure 3. Input reactance for a circular cavity as a function of feed probe length.

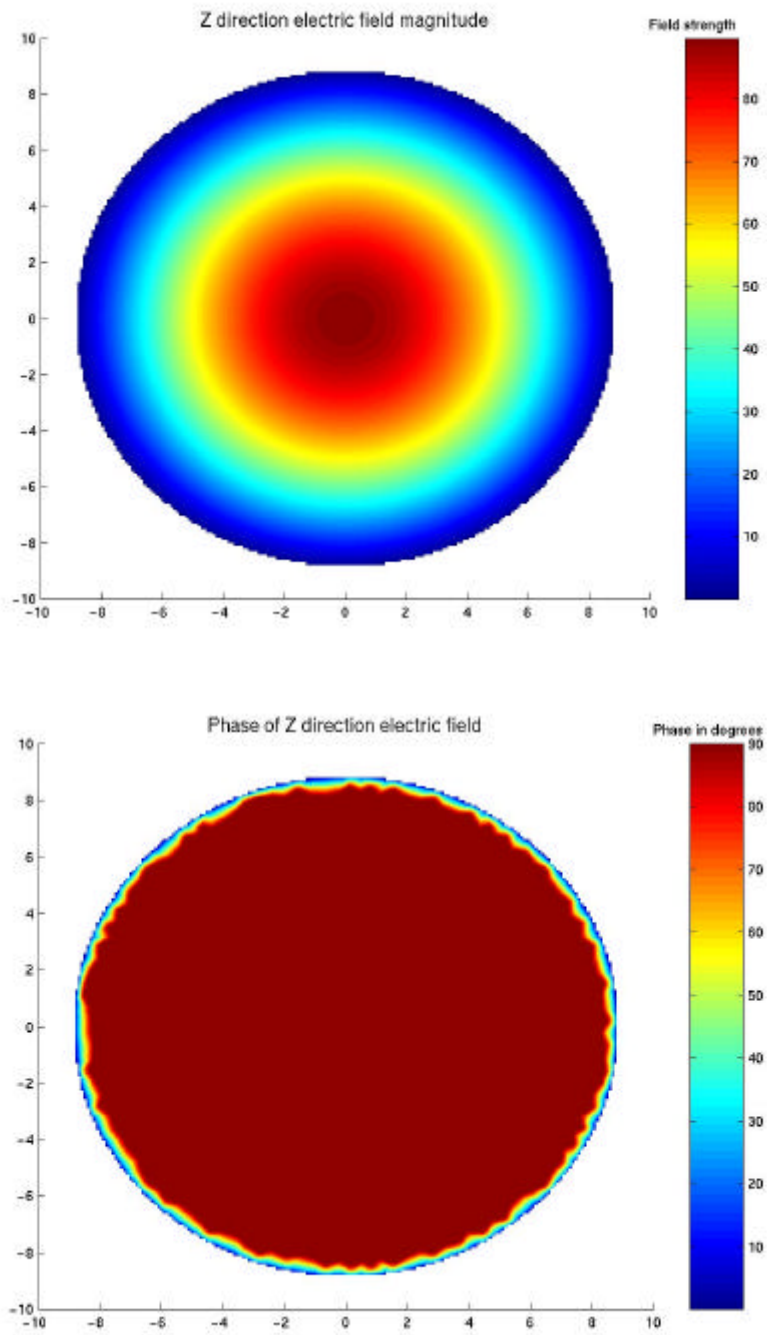


Figure 4. Magnitude and phase of the axial field at the base of the cavity.